THEORY OF ELECTRON CYCLOTRON RESONANCE HEATING II:

LONG TIME AND STOCHASTIC EFFECTS

by

M. A. Lieberman and A. J. Lichtenberg

Memorandum No. ERL-M306

10 September 1971

Electronics Research Laboratory

College of Engineering
University of California, Berkeley
94720

THEORY OF ELECTRON CYCLOTRON RESONANCE HEATING II: LONG TIME AND STOCHASTIC EFFECTS

M. A. LIEBERMAN and A. J. LICHTENBERG

Department of Electrical Engineering and Computer Sciences
and the Electronics Research Laboratory,
University of California, Berkeley, California 94720

ABSTRACT

The theory of single particle electron cyclotron resonance heating in a magnetic mirror is treated analytically and numerically, from the viewpoint of (a) an impulsive heating approximation and (b) a stochastic approximation, using a Fokker-Planck equation. Using (a), numerical calculations of particle heating are performed for $\sim 10^5$ half-bounce times τ_b. Numerically and analytically from (a), for a given rf field strength, we obtain two limiting energies W_s and W_b, with $W_b \simeq 5W_s$. For the transverse particle energy at resonance $W_{\perp R} < W_s$, invariant curves do not exist, the random phase assumption holds, and the particle heating is stochastic, described by a Fokker-Planck equation as in (b). For $W_s < W_{\perp R} < W_b$, invariant curves and stochastic regions coexist; the Fokker-Planck equation is inappropriate. For $W_{\perp R} > W_b$, invariant curves exist which form a barrier to further particle heating. For a parabolic mirror $B(z) = B_0(1+z^2/L^2)$ with cyclotron resonance at $z = \pm \ell$, $W_b = 1.85eEL(1+\ell^2/L^2)^{1/2}(\tau_b/\tau_s)^{2/3}$, where e is the electronic charge, E the rf electric field, and τ_s is the period for the cyclotron phase to slip 2π with respect to

the rf field. This result is in good numerical agreement with exact calculations, and with the results of a Hamiltonian approximation. In (b), we obtain the Fokker-Planck coefficients from (a), and solve the Fokker-Planck equation numerically and analytically. If the effective time spent in resonance per half-bounce $\tau_e \propto v_{\perp R}^{-P}$ (Analytically and from exact numerical calculations, $P \simeq 2/3.$), the particle distribution function $g(v_{\perp R},t) \propto (v_{\perp R}^{2P}/t)\exp - [Kv_{\perp R}^{2P+1}/t]$, where $\frac{1}{2} mv_{\perp R}^2 = W_{\perp R}$ and t is the time. The average particle energy $\langle v_{\perp R}^{\ 2} \rangle \propto t^{1/(4P+2)}$. Analytic results are in agreement with exact numerical calculations.

1. INTRODUCTION

It has long been recognized that particles confined in a magnetic mirror can be efficiently heated by an rf field which resonates with the particle gyrofrequency somewhere in the mirror region. In a companion paper (JAEGER et al, 1971), hereafter referred to as I, previous approaches to the analysis of this resonance heating were presented. In I, the equations of motion for the particle were solved in the vicinity of the resonance region, obtaining the result that for particles turning in the resonant zone, the effective time t_e spent in resonance per half-bounce time τ_b scaled with the transverse velocity at resonance $v_{\perp R}$ as $v_{\perp R}^{-P}$, where $P = 2/3$ analytically and $P \simeq 0.5\text{-}0.7$ from exact numerical calculations.

It is also well known that for sufficiently weak rf fields and high particle energies, the particle is not heated, but rather its energy oscillates on a time scale long compared to τ_b. This oscillation is due to the appearence of an adiabatic invariant of the particle motion. The study of this behavior and the transition from heating to energy oscillation was the principal topic of I. Transforming the exact equations of motion to a Hamiltonian approximation, and using the method of resonance breakdown of adiabatic invariance due to secondary island formation, a criterion for the rf field necessary to destroy the invariant at a given energy was obtained; i.e., for a given rf field, the maximum energy to which particles can be heated was found to be given by (70) in I.

The transition between stochastic heating and oscillatory energy changes for cyclotron heating is closely allied to a wide class of problems in which particles are subject to periodic impulsive forces.

In a previous paper (LIEBERMAN and LICHTENBERG, 1971), this transition was explored theoretically and numerically for the Fermi problem of a ball bouncing between a fixed and a vibrating wall. In that case, exact solutions of the motion are attainable over a single bounce period. This permits numerical investigation of the motion over hundreds of thousands of collisions with the wall, and thus a statistical description of the distribution of particle energies is obtainable numerically. A particular model of cyclotron heating, in which the resonant heating was approximated by a constant velocity impulse in time, was treated by the same method, both to show an application of the method and to investigate certain differences in the results for the case in which the mapping of the single bounce transformation is not area preserving, as compared to the Fermi problem, in which the mapping is area preserving.

In Section 2 of this paper, the approximations required to obtain an impulsive heating model are considered. The mapping equations relating the velocity and phase of the particle at successive resonance crossings are derived for an arbitrary power law dependence of t_e on $v_{\perp R}$. The phase space of the particle is explored numerically for hundreds of thousands of collisions, and the stability of the fixed points in the phase plane is examined. From these considerations, for a fixed rf field strength, the barrier to particle heating is derived. The results obtained are in substantial agreement both with the Hamiltonian approximation of I and with exact numerical solutions. The averaging and expansion procedure in the Hamiltonian approximation results in mappings between resonances that are area preserving and thus different

in character from the impulse approximation. However, despite this fundamental difference, the results are quite similar in most important respects.

In Section 3 of this paper, the cyclotron resonance heating of particles is considered using a stochastic theory. The appropriate Fokker-Planck equation, valid in the stochastic region of phase space, is obtained, with the Fokker-Planck coefficients being calculated from the mapping equations. The Fokker-Planck equation is solved numerically and analytically, to obtain expressions for the evolution of the velocity distribution function and the increase in average energy with time. The results agree with exact numerical orbit calculations and with observations of heating in a pulsed, electron cyclotron heating experiment (LICHTENBERG et al, 1969).

2. IMPULSE APPROXIMATION

A. Model and Validity

As a simple cyclotron heating model, we consider a general mirror magnetic field $B_z(z)$, with a minimum at $z = 0$, as shown in Fig. 1a. The rf heating zones consist of two circularly polarized electric fields lying in the x-y plane, of small longitudinal extent located at $z = \pm \ell$, and rotating at the local cyclotron frequency. The guiding center approximation is used to describe the particle motion for $|z(t)| \neq \ell$. As the particle is reflected back and forth in the mirror, it passes through the heating zones at $z = \pm\ell$. The motion of the particle, assuming an impulsive transverse force in the heating zone, and assuming that the longitudinal velocity of the particle is zero at $|z| = \ell\pm$, is described by a

set of difference equations relating the transverse velocities on successive collisions to the impulsive force. From the conservation of transverse momentum, we obtain the equation for the transverse velocity change

$$v_{n+1} = (v_n^2 + V^2 + 2v_n V \cos \theta_n)^{1/2}, \tag{1}$$

where v_n is the magnitude of the transverse velocity of the particle just before a collision with the heating zone, n is the number of collisions with the heating zone, θ_n is the angle between the rf electric field and the transverse velocity vector of the particle just before a collision, and V is the magnitude of the velocity increment with the rf field imparts to the transverse velocity of the particle. The geometrical relation between the various velocities is given in Fig. 1b. We note that the energy gain described by (1) shows both a phase-independent term V^2 and a phase-dependent term $2v_n V \cos \theta_n$.

The change in the phase angle θ between successive collisions is given by

$$\theta_{n+1} = \theta_n + \Delta\theta_b + \Delta\theta_i, \tag{2}$$

where $\Delta\theta_i$ is the impulsive phase slippage due to the particle-field interaction and $\Delta\theta_b$ is the phase slippage which occurs during the time interval τ_b between successive collisions. The angle $\Delta\theta_i$ is obtained from conservation of transverse momentum (see Fig. 1b) as

$$\Delta\theta_i = \mathrm{Sin}^{-1} \left(\frac{V \sin\theta_n}{v_{n+1}} \right), \; v_n \geq - V \cos \theta_n$$

$$= \pi - \mathrm{Sin}^{-1}\left(\frac{V\sin\theta_n}{v_{n+1}}\right), \quad v_n < V\cos\theta_n. \tag{3}$$

The angle $\Delta\theta_b$ is found by integrating the phase slippage of the particle over a bounce time:

$$\Delta\theta_b = \int_0^{\tau_b} [\omega_o - \omega_o(z(t))]dt, \tag{4}$$

where ω_o is the frequency of the applied field, $\omega_c(z) = eB_z(z)/m$, and $z(t)$ is the axial position of the particle. If the longitudinal particle velocity is zero at $|z| = \ell+$, it is easily seen that $\Delta\theta_b \propto v_{n+1}^{-1}$. Introducing a large dimensionless parameter M, we write

$$\Delta\theta_b = 2\pi M(V_o/v_{n+1}), \tag{5}$$

where V_o is a characteristic velocity to be defined subsequently. For a parabolic mirror,

$$\omega_c(z) = \omega_{co}(1+z^2/L^2), \tag{6}$$

and τ_b is the half-bounce time in the mirror, given by (see (6) in I)

$$\tau_b = \pi(\ell^2 + L^2)^{1/2}/v_n, \tag{7}$$

where v_n is the transverse velocity at the resonance plane. The axial position is given by $z(t) = \ell\cos(\pi t/\tau_b)$, from which (4) is integrated to yield

$$M = \omega_{co} \ell^2 (\ell^2 + L^2)^{1/2} / (4L^2 V_o). \tag{8}$$

The heating of particles near the point of resonance in a mirror was studied in Section 2B of I, where it was shown that the heating occurs in a zone of width w which is much smaller than the scale length of the dc magnetic field variation. The particle interacts with the rf field in the zone for a time t_e which is much shorter than the half-bounce time τ_b. These considerations demonstrate that the concept of an impulsive heating zone is valid. This result of heating in a localized zone was also obtained by GRAWE (1969), even though he then calculated the heating over an entire half-bounce τ_b of the particle, assuming that the particle's parallel velocity v_z was unperturbed by the rf field. In contrast, in the above model, the particle's parallel velocity, measured at the center of the mirror, is perturbed by the rf field, since a portion of the perpendicular energy gained or lost at the resonant zone is transformed into a corresponding parallel energy gain or loss by the mirror field.

From the results of Section 2B in I, we write

$$V = \frac{e}{m} E \, t_e, \tag{9}$$

where $E = 2|E_\perp|$ is the magnitude of the applied field at the resonance zone, and t_e is the effective time the particle spends in resonance. We distinguish two different forms for t_e, depending on the nature of the particle's trajectory. For particles which pass with constant axial velocity through the resonant zone, we write, from (22) in I,

$$t_e \approx 1.13 \left(\frac{2}{|\alpha v_{zR}| \omega} \right)^{1/2}, \tag{10}$$

where $\alpha = B_z^{-1}(dB_z/dz)_\ell$, v_{zR} is the parallel velocity at the resonant plane, and ω is the rf driving frequency. We note that V is independent of the transverse velocity at resonance v_n. We expect this result to hold initially, provided $v_{\perp R} \sim v_{zR} > > V$. In this weak rf field approximation, a particle may slowly gain transverse energy in a stochastic fashion, while continuing to turn far from the resonant zone. However, eventually, the particle will begin to turn in the resonance zone, and (10) becomes invalid.

In the more usual experimental situation, one has $v_{\perp R} \sim v_{zR} \leq V$ initially; i.e., a strong rf field is applied. On the first pass through resonance, the phase-independent term of (1) dominates, such that the transverse energy of all particles is greatly increased. The particles immediately begin to turn in the resonant zone, so that (10) applies at most to the first pass through resonance. From (23) in I, we then have

$$t_e = .71\omega^{-1} \left(\frac{2\omega}{\alpha v_n} \right)^{2/3}. \tag{11}$$

In this case, we find $V \propto v_n^{-2/3}$, so that as a particle's perpendicular energy is increased, the heating becomes less and less effective.

It is convenient to treat (10) and (11) together, by writing

$$V = V_o (V_o/v_n)^P, \tag{12}$$

where an arbitrary power P has been introduced, and the normalizing velocity V_o is independent of v_n. Defining a normalized perpendicular velocity $u_n = v_n/V_o$ and using (9), we re-write (1) and (2) as

$$u_{n+1} = (u_n^2 + 2u_n^{1-P}\cos\theta_n + u_n^{-2P})^{1/2} \tag{13}$$

$$\theta_{n+1} = \theta_n + \Delta\theta_b + 2\pi M/u_{n+1}, \tag{14}$$

where

$$\Delta\theta_b = \mathrm{Sin}^{-1}(u_{n+1}^{-1-P}\sin\theta_n),\ u_n^{1+P} \geq -\cos\theta_n$$
$$= \pi - \mathrm{Sin}^{-1}(u_{n+1}^{-1-P}\sin\theta_n),\ u_n^{1+P} < -\cos\theta_n. \tag{15}$$

In this section, we study the difference equations (13)-(15) for the case (10) of V constant (P=0), in some detail, both computationally and analytically. Where appropriate, we also discuss these equations for the case of (11), for which P = 2/3.

B. Numerical Calculations

The difference equations (13)-(15) are readily solvable, for hundreds of thousands of bounces in the mirror on a high speed computer. To explore the entire phase space $(u,\phi=\theta \mathrm{Mod} 2\pi)$ of the electron, we divide the phase interval $(0,2\pi)$ into 100 increments and the velocity interval $(0,u_{max})$ into 200 increments. We keep track of the number of times a particle is found within any of the 20,000 cells of the phase space. Numerical calculations of this type have previously been made (LIEBERMAN and LICHTENBERG, 1971). The results of the calculations for the electron cyclotron heating problem, with P=0 and M = 57.8, for ten particles,

are given in Fig. 2, after (a) 2560 and (b) 5120 collisions per particle. Normalized velocity u is measured downward. A symbol in each cell is used to represent the number of cell occupations, with a blank meaning zero occupations. The particles are initially given phases and low velocities, chosen randomly. Subsequent bounces in the mirror allow them to explore the phase space available. Generally, low occupation numbers at low velocities are seen, indicating the presence of a strong frictional force which accelerates particles to higher energies. It is clear from the form of the phase plane and the way it changes with the number of collisions, that there exist points in the phase plane which are sinks for particles. The centers of these sinks are "spiraling-in" singularities in the phase plane, as will be shortly described. Particles placed near such a point will in their subsequent motion orbit around the point, slowly spiraling-in toward the singularity and becoming trapped.

From extensive numerical computations using the impulsive heating approximation, one generally observes the presence of three distinct regions in velocity space. In a low velocity region $u < u_s$, the spiraling-in orbits do not exist; the particle motion appears to be stochastic in nature. In an intermediate velocity range, the particle sinks exist and the particle motion is not stochastic in the neighborhood of the sinks. Not all particles with initially low velocities become trapped in the sinks; some penetrate into a high velocity range and the particles then appear to be slowly heated in a regular, nonstochastic manner. These effects can be seen in Fig. 2, for which $u_s = 9.5$. Of the ten particles started at low velocities, one has been trapped in a double sink at $u = 12$, four in a sink at 28.9, and one in the sink (main island) at $u = M = 57.8$. The

other four particles have penetrated above u = M; their velocities are observed to continuously increase in a non-stochastic fashion.

The qualitative features of the phase space are retained for arbitrarily large values of M and all values of $P \geq 0$. In Fig. 3 we give results for P = 0, but with M = 578. There are twenty particles with (a) 320, (b) 640, (c) 1280, and (d) 2560 collisions per particle. The corresponding distribution of particle velocities $\bar{f}(u) = \sum_{o}^{n} d\phi f(u,\phi,n)$, summed over phases and the total number of collisions, is shown in Fig. 4. We again see the striking feature of particle sinks (at arrows) for $u > u_s$ (= 30.1 for this case). (For larger u's, the arrows point to low density regions, since the particles are orbiting around these regions and have not yet spiraled in to the singular points.)

Fig. 5 shows the result of further calculations to investigate the energy increase of the particles as a function of collision number n. We plot the maximum particle velocity u_{max} of a group of twenty particles as a function of n, for M = 578. One sees a fairly rapid heating of particles below u_s, followed by a slower heating which sets in somewhat above u_s.

Fig. 6 shows the average energy $\langle u^2 \rangle$ as a function of n for M = 578, in the stochastic region $n \lesssim 160$ for which $u_{max} < u_s$. We can estimate the heating rate of the particles as follows: From the figure, $\langle u^2 \rangle \propto n$. But $n \propto ut$, where t is the time (Higher velocity particles collide faster than lower velocity particles). Combining the two proportionalities, we have $\langle u^2 \rangle \propto t^2$, or a heating rate

$$\frac{d\langle u^2 \rangle}{dt} \propto t. \tag{16}$$

This proportionality is in agreement with the results of the stochastic theory given in Section 3. As will be seen there, if V is a function

of $v_{\perp R}$ given by (12), rather than constant as used in the numerical calculations, $\langle u^2 \rangle$ depends on t as $\langle u^2 \rangle \propto t^{2/(2P+1)}$.

In a previous paper (LIEBERMAN and LICHTENBERG, 1971) similar numerical calculations were made as an aid in understanding the Fermi acceleration mechanism. For Fermi acceleration, one finds unoccupied islands in the phase plane, bounded by adiabatic curves, and therefore inaccessible from outside. The centers of the islands are elliptic singularities in the phase plane. Near these centers, the particle motion traces out closed trajectories, rather than spiraling-in orbits. One finds a stochastic transition velocity u_s, below which all singularities are hyperbolic, so that unoccupied islands do not exist below u_s. In addition, an impenetrable barrier velocity u_b generally exists, above which initially low velocity particles can never be heated. The Hamiltonian model of cyclotron resonance heating in I, Section 3 shares the characteristics of Fermi acceleration: the existence of unoccupied islands in the phase plane bounded by invariant curves, and the existence of invariant curves which drift across the phase plane, thus bounding the energy gain. The difference between the impulsive model in this section and the Hamiltonian model of I that accounts for the differences in the trajectory behavior, rests on the fact that the phase space mapping of the impulsive model is not area-preserving. The mathematical exposition is given in the following section.

C. Linear and Nonlinear Stability

The technique for analytically examining the linear aspects of the electron cyclotron heating problem is the following: determine the fixed

points in the phase plane and examine the stability of the linearized motion about these singularities. Equations (13)-(15) define a mapping in a two-dimensional space $\underset{\sim}{p} = (u,\phi)$, such that $\underset{\sim}{p}_{n+1} = M(\underset{\sim}{p}_n)$, which can be iterated: $\underset{\sim}{p}_{n+k} = M^k(\underset{\sim}{p}_n)$. The condition that the mapping is area-preserving is that $\mathrm{Det}(J) = 1$. Here $J(\underset{\sim}{p}_n) = J(u_{n+1},\phi_{n+1}|u_n,\phi_n)$ is the Jacobian matrix of the mapping.

It is well-known that a dynamical system describable by a Hamiltonian $H(q_1\cdots q_n,p_1\cdots p_n,t)$ induces in the 2n-dimensional phase space of the system an area(measure)-preserving flow. In general, however, for a three-dimensional Hamiltonian, the flow in a restricted space of two dimensions is not area-preserving. The approximation to cyclotron resonance heating given by (13)-(15) is an example of such a non-area-preserving mapping. It should be noted, however, that in the Hamiltonian approximation of I, sufficient invariants exist to recover the area-preserving property.

Fixed Points and Stability. A mapping possesses a fixed point of order k at $\underset{\sim}{P} = (u,\phi)$ when $\underset{\sim}{P} = M^k(P)$ and $\underset{\sim}{P}$ is not a fixed point of any order less than k; i.e., a particle located exactly at $\underset{\sim}{P}$ will re-appear after k collisions. For every positive integer value of k, there is a denumerably infinite set of fixed points. Fixed points of order k occur in families of exactly k members each.

To obtain all the k^{th} order fixed points, we solve the 2k+2 algebraic equations:

$$\underset{\sim}{P}_{j+1} = M(\underset{\sim}{P}_j),\ j = 1,\ldots k; \qquad (17)$$

$$\underset{\sim}{P}_{k+1} = \underset{\sim}{P}_k .$$

For the k = 1 fixed points of (13)-(15), we obtain

$$[u_1,\phi_1] \simeq [M/m, \frac{1}{2}\pi + \frac{1}{2}(m/M)^{1+P}] \tag{18}$$

and

$$[u_1,\phi_1] \simeq [M/m, \frac{3}{2}\pi - \frac{1}{2}(m/M)^{1+P}], \tag{19}$$

$m = 1,2,3,\cdots$, valid in the limit $u_1 >> 1$. There are two fixed points for each integer value of m. These are the significant fixed points, as can be seen from Figs. 2 and 3.

To investigate the stability of the particle motion in the immediate neighborhood of a fixed point $\underset{\sim}{P}_1$ of order k, we introduce a linearized mapping L by

$$\Delta\underset{\sim}{p}_{n+k} = L \cdot \Delta\underset{\sim}{p}_n, \tag{20}$$

where $\Delta\underset{\sim}{p}_n = \underset{\sim}{p}_n - \underset{\sim}{P}_1$. L is equal to the ordered product of k Jacobian matrices of M, each evaluated at the k successive fixed points of the family of which $\underset{\sim}{P}_1$ is a member: $L = J(\underset{\sim}{P}_k)\, J(\underset{\sim}{P}_{k-1}) \cdots J(\underset{\sim}{P}_1)$. Under successive iterations of L, the particle moves in an orbit near the fixed point. To determine the character of the orbit, we solve the two linear difference equations (20) by introducing $\Delta\underset{\sim}{p}_{n+qk} = \Delta\underset{\sim}{p}_0 r^q$. We obtain the following characteristic equation for r:

$$r^2 - r\,\mathrm{Tr}\,L + \mathrm{Det}\,L = 0. \tag{21}$$

It is well known that the quantities Tr L and Det L are invariant, independent of the cyclic order of the k Jacobian matrices comprising L.

Thus the roots of (21), are the same for all k fixed points in a given family.

The character of the two roots of (21) have been studied extensively in connection with non-linear mechanics (STOKER, 1950). For $0 < \frac{1}{4} (\text{Tr } L)^2 < \det L < 1$, these roots are complex conjugates, having a magnitude less than unity. The particle than spirals in toward the central fixed point ("trapped orbit"). Such orbits are responsible for the particle "sinks" seen in Figs. 2 and 3. For $-1 + |\text{Tr } L| < \det L < \frac{1}{4} (\text{Tr } L)^2 < 1$, a trapped orbit is also obtained, with the particle moving in toward the fixed point in a non-spiraling orbit. For $\det L > \frac{1}{4} (\text{Tr } L)^2 > 1$, complex conjugate roots having a magnitude greater than unity are obtained (unstable, spiraling-out motion). All other cases result in two real roots, one of which has a magnitude greater than unity. The orbit is then unstable.

For the k = 1 fixed points in (18) and (19), we obtain Tr L and Det L as:

$$\text{Tr } L = 2 \pm 2\pi m^{P+2}/M^{P+1} + O(u_1^{-2P-2})$$
$$\text{Det } L = 1 - \frac{1}{2} (P+2)(m/M)^{2P+2} + O(u_1^{-4P-4}), \qquad (22)$$

where the positive sign refers to the fixed point near $\phi_1 = \pi/2$ and the negative sign to the fixed point near $3\pi/2$. From the above stability conditions, we find that the former fixed point is always unstable, while the fixed point near $3\pi/2$ has trapped orbits (particle spirals into the fixed point) provided $m^{P+2} < (2/\pi)M^{P+1}$. Substituting $m = M/u_1$, we find $u_1 > u_s$ for trapped orbits, where

$$u_s = \left(\frac{1}{2}\pi M\right)^{1/(2+P)} . \tag{23}$$

The particle circles the singular point, making a complete rotation every $2\pi/\Delta\hat{\theta}$ bounces, where, for $u_1 >> u_s$,

$$\Delta\hat{\theta} = (2\pi M)^{1/2}/u_1^{1+P/2}. \tag{24}$$

At the same time, for $u_1 > u_s$, the particle slowly spirals exponentially in toward the singular point as $\exp(-\beta n)$, where the spiraling-in rate is

$$\beta = \frac{1}{4}(P+2)u^{-2P-2}. \tag{25}$$

These trapped orbits can be seen in Figs. (2) and (3).

Stochastic transition velocity.-- Extensive numerical calculations of the difference equations (13)-(15) show the existence of a transition velocity u_s, below which no trapped orbits are observed, and all phase space states are accessible to low velocity particles. Above u_s, disjoint areas in phase space exist, with only one-way access among these areas. Since a minimal requirement for a stochastic description of particle motion in a given region of phase space is that all positions in phase space be accessible and have access to all other positions, we refer to u_s as a stochastic transition velocity; below u_s, a stochastic description of the motion is possible, as described in Section 5.

To calculate the value of u_s, one must in principle examine the character of the orbits around families of fixed points of all orders k. However, numerical computations and analytical results for both

area-preserving and non-area-preserving mappings suggest that the stochastic barrier u_s is associated with the stability or instability of the k = 1 fixed points; namely, u_s is in fact given by (23).

A physical interpretation of the transition velocity u_s can be obtained by observing that the stability boundary occurs when the phase shift per bounce of the island oscillation around the fixed points is equal to π. This is just the well known condition for stop bands in a periodic structure. In terms of the period $\tau_i = 2\pi/\Delta\hat{\theta}$ of the island oscillation, $\tau_i < 2\tau_b$ for stochasticity, where τ_b is the time between collisions.

Non-area-preserving character and absolute barrier. -- The fact that Det L differs from unity by a small term, of order u^{-2P-2}, suggests that the features of area-preserving mappings ought to be present for the mapping (13)-(15) in an approximate way, weakly perturbed by the non-area-preserving character of the mapping. In particular, we expect to see some manifestation of the impenetrable velocity barrier u_b, which is exactly present for sufficiently smooth, area-preserving mappings, as described in LIEBERMAN and LICHTENBERG (1971). This barrier curve, is the Arnol'd-Moser invariant curve of the mapping having the lowest average value of u. ARNOL'D (1963) and MOSER (1962) have shown that, given suitable smallness conditions on the Jacobian derivatives of the mapping, invariant curves always exist. However, in practice, these existence proofs are of little use in predicting the location u_b of an absolute barrier (MOSER, 1962).

To estimate the location of u_b, we expand (13)-(15) for large u, keeping only the dominant terms. We discuss the case of a constant

velocity impulse (P=0) in some detail, and the case P > 0 only in qualitative terms. Performing the expansion for P = 0, we find

$$u_{n+1} \approx u_n + \cos \theta_n$$
$$\theta_{n+1} \approx \theta_n + 2\pi M/u_{n+1}. \tag{26}$$

These equations describe an area-preserving mapping, which has been treated previously (LIEBERMAN and LICHTENBERG, 1971A). We found in that case that u_b was bounded from below by $(\pi M)^{1/2}$ and that an approximate Hamiltonian treatment of these equations yielded $u_b \approx 2.8M^{1/2}$. We expect little change in the location of this barrier due to the non-area-preserving properties of the exact equations (13)-(15), since for $u \approx u_b$, the area-preserving property is approximately satisfied; eg, from (22) for M = 578, det L differs from 1 by less than 0.1%. However, we expect an important change in the nature of the barrier; the numerical calculations of Figs. 2 and 3 show that u_b is no longer an absolute barrier, but represents a velocity above which the particle heating rate suddenly decreases. The transition to this slow form of energy gain, can be seen as the "kink" in the curve of Fig. 5.

The location of the barrier velocity u_b has not been obtained analytically for the case of P > 0. In particular, the important case in most experiments of P = 2/3, corresponding to the turning of particles in the resonance zone, has not been considered. However, one generally finds in problems of this type (see JAEGER and LICHTENBERG, 1971) that $u_b \approx C\, u_s$, where $C \approx 2.2$. This result seems reasonable, since as u is increased from low toward high values, one expects the onset of linear

stability at u_s to be shortly followed by the onset of nonlinear stability associated with the Arnol'd-Moser curve at u_b.

D. Criteria for Stochasticity

We now consider the conditions under which particles in a magnetic mirror are stochastically heated by the applied rf field. For convenience, the parabolic field (6) is used. The breakdown of stochasticity is associated with the existence of invariant curves in the phase plane which isolate regions in phase space.

Particles turn far from resonance. -- The case of a weak applied rf field is first examined, for which $v_{\perp R} \sim v_{zR} >> V$ initially, and V is given by (9) and (10) and is independent of transverse energy. From the stability condition (23), setting P = 0 and introducing the factor C, we determine the ordering of the natural periods for stochasticity,

$$\tau_b > \frac{4}{\pi C^2} \tau_s \frac{v_{\perp R}}{V}, \tag{27}$$

where, for the parabolic field,

$$\tau_s = \frac{2\pi}{\omega_{co}} \frac{L^2}{\ell^2} \tag{28}$$

is the period for the phase of the particle to slip 2π radians with respect to the rf field, averaged over a half-bounce time τ_b. Substituting for τ_b from (7), we obtain the stochasticity condition on the particle energy

$$W_{\perp R} < \frac{C^2\pi^2}{4} eEL(1+\ell^2/L^2)^{1/2} t_e/\tau_s, \tag{29}$$

where $W_{\perp R}$ is the electron transverse energy at the resonant point. Using $\alpha = 2\ell(\ell^2+L^2)^{-1/2}$ and $\omega = \omega_{co}(1+\ell^2/L^2)$ in (10), we find that $t_e = 1.13\ L(\ell v_{zR}\omega_{co})^{-1/2}$.

It is important to note that (29) is valid only if the particle continues to turn far from the resonance zone at the stochastic barrier itself. From (12), we obtain the necessary condition as

$$eE \leq 2.25(C\ell)^{-2}(\ell^2+L^2)^{1/2} W_{zR} \tag{30}$$

where $W_{zR} = \frac{1}{2} mv_{zR}^2$.

To illustrate consider $f_{co} = 10^{10}$ GHz, $\ell = L = 10$ cm, and $v_{zR} = 10^8$ cm/sec (2.7 eV). In view of (30), we choose E = 0.1 V/cm, an exceedingly weak field. Then $\tau_s = 10^{-10}$ sec, and $t_e = 14.3\ \tau_s$. From (9), $V = 2.5\text{x}10^5$ cm/sec, so that the initial condition $v_{\perp R} \sim v_{zR} > > V$ for the validity of (10) is satisfied. Setting $C \simeq 2.2$ in (29), we obtain the stochasticity condition $W_{\perp R} < 250$ eV.

Particles turn in the resonant zone. -- It should be clear from the above considerations that for usual experimental conditions, particles begin to turn in the resonant zone after one or a few bounces. In this case, t_e is given by (11) rather than (10), and $V \propto v_{\perp R}^{-2/3}$. Setting P = 2/3 and introducing the factor $C \simeq 2.2$ in the stability condition (23), we obtain the ordering of the natural periods for stochasticity

$$\tau_b > \frac{4}{\pi C^{8/3}}\ \tau_s\ \left(\frac{v_{\perp R}}{V_o}\right)^{5/3}, \tag{31}$$

where from (9), (11) and (12),

$$V_o = (.71 \frac{e}{m} E)^{3/5} (\ell^2+L^2)^{1/5} (\frac{\tau_s}{2\pi})^{1/5} . \quad (32)$$

If (32) is substituted into (31), the stochasticity condition for the particle energy may be written as

$$eEL > \frac{4^{5/3}}{.71\pi C^{8/3}} (1+\ell^2/L^3)^{-1/2} (\tau_s/\tau_b)^{2/3} W_{\perp R}. \quad (33)$$

Finally, eliminating τ_b through the use of (7), we cast (31) in a convenient form for estimating the peak energy that can be obtained with a given rf field as

$$W_{\perp R} < .24C^2 eEL(\bar{t}/\tau_s)^{1/2}, \quad (34)$$

where

$$\bar{t} = (\frac{m}{eE})^{1/2} L^{1/2} (1+\ell^2/L^2)^{5/4} \quad (35)$$

is a field-dependent time.

E. Comparison of Impulse and Hamiltonian Approximations with Exact Equations

To check the impulse and Hamiltonian approximations we compare the results of the two theories with the results of an exact orbit calculation. This check can be accomplished very accurately on the time scale of a single energy oscillation. On longer time scales the exact numerical calculations become computationally very time consuming. For our numerical calculation we choose parameters such that for constant V(P=0), M = 30 and u ≃ 15,

corresponding roughly to the m = 2 resonance. For these parameters the trajectory is clearly in the adiabatic region of phase space (according to both theories), and the spiraling in, if it exists, should be marginally measurable. In Fig. 7, we give the phase space plot of resonance crossings (numbered points) for 100 crossings counted for increasing $|z|$ only. The calculation took approximately 10 minutes on a CDC 6400 computer. The frequency of the energy oscillation was nearly an integer, such that the number of resonance crossings per island oscillation, $\tau_i/\tau_b \approx 10$. The measured $u \approx 17.5$.

We can compare the amplitude and frequency of the energy oscillation in Fig. 7 with the approximate calculations. For convenience we choose $P = 0$ and $u = u_o >> 1$, so that (13)-(15) reduce to (26). These equations have previously been treated in a Hamiltonian limit (LIEBERMAN and LICHTENBERG, 1971). The Hamiltonian is

$$H = \frac{2\pi M}{u_o^2}\frac{\hat{u}^2}{2} + \sin\theta = \text{const}, \tag{36}$$

where $\hat{u} = u - u_o << u_o$. The frequency for the linearized motion near the singular point is

$$\Omega_o = (2\pi M)^{1/2}/u_o^2, \tag{37}$$

and the amplitude is

$$\hat{u} = \frac{u_o}{(2\pi M)^{1/2}}(\sin\theta - \sin\theta_1)^{1/2} \tag{38}$$

where θ_1 is the value of θ for which $\hat{u} = 0$. For the Hamiltonian theory

of electron cyclotron heating, we use I, (63) and (65), and to account for the nonlinear phase excursion modify I, (46) to

$$\Delta P = (F/G)^{1/2}(\cos\phi - \cos\phi_1)^{1/2}.$$

In the impulse approximation we take $M = 30$, $u_o = 17.5$, and $\theta_1 = \pi/2$, and for the Hamiltonian approximation $N = 2$, $P_2 = 9.6P_1$, $f_n \simeq 1/2$, $P_1 \simeq 1.2\times10^{-3}$, $\epsilon = 4\times10^{-4}$, $\phi_1 = 0$ and $\Delta w = 1.77\ \Delta P_1$. With these values, the number of collisions per island oscillation $\tau_i/\tau_b = 2\pi/\Omega_o$ and the peak energy excursion $\Delta W_{max}/W_o$ are compared below.

	τ_i/τ_b	$\Delta W_{max}/W_o$
Numerical	10	.2
Impulse	7	.2
Hamiltonian	6-7	.25

Including the effect of the nonlinearity, τ_i/τ_b would be increased by approximately 15% for both the impulse and Hamiltonian theories.

We now compare the stochasticity boundary from I, (71), derived from the Hamiltonian approximation with the stochasticity boundary from (34) derived from the impulse approximation for $P = 2/3$. These expressions are similar but not identical. Putting $C \simeq 2.2$ in (34), we note that the ratio

$$\frac{W_{\perp R}(\text{impulse})}{W_{\perp R}(\text{Hamiltonian})} = \left(\frac{eE\tau_{co}^2 L^3}{m\ell^4}\right)^{1/12} (1+\ell^2/L^2)^{7/24}, \qquad (39)$$

which is a very slowly varying function of the parameters. As an example,

for an electron cyclotron experiment previously reported (LICHTENBERG et al, 1969), we have $\tau_{co} \simeq 10^{-10}$sec, $E \simeq 10^3$ V/cm, $\ell \simeq 7.5$ cm and $L \simeq 15$ cm. The ratio in (39) is then 0.77, which implies a good agreement between the theories. For this example, condition (34) yields $W_{\perp R} < 54$ keV, while (71) in I yields $W_{\perp R} < 70$ keV.

We can also compare the stochasticity condition (34) with that of I, (71) and with exact numerical calculations. To do this we repeat the numerical calculation for a field twice as large and four times as large as that in Fig. 7. The invariants exist at twice the field, but at four times, the orbit is ergodic. For a fixed particle energy, we obtain the following comparison:

	Stochasticity field ε (normalized)
Numerical	$8\text{x}10^{-4} > \varepsilon > 4\text{x}10^{-4}$
Impulse	$\varepsilon \simeq 4.9\text{x}10^{-4}$
Hamiltonian	$\varepsilon \simeq 6.4\text{x}10^{-4}$

Both the impulse and Hamiltonian theories are in good agreement with the exact orbit calculations.

The one important difference between the Hamiltonian and impulse approximations is, of course, the question of whether or not the mappings are area-preserving. Although the difference between area-preserving mappings, as embodied in the Hamiltonian theory of I, and the non-area-preserving mappings of the present section seems to be of importance in determining an absolute limit to electron cyclotron heating, this difference may not be of much practical significance. As an example, consider the

case of a particle turning in the resonance zone, for which P = 2/3, and set M ≈ 200, a typical experimental value. From (23), one finds u > 8.6 for spiraling-in orbits to exist. From (25), one then obtains the spiraling-in rate as $\beta < .001$; ie, it would characteristically take a few thousand collisions for the particle to spiral in to the singular point. Also, Det L differs from unity by an exceedingly small amount, 0.1%, so one would expect the heating of a particle to slow tremendously as it crossed the barrier u_b.

Rather than being of practical significance, the difference in area-preserving character between the Hamiltonian and impulse formulations may shed light on the validity of the assumptions of each theory. For example, the Hamiltonian theory treats the rf field as a first-order perturbation, such that the total Hamiltonian is linear in the applied rf field strength. In contrast, the impulse theory treats the particle-field interaction to all orders in the rf field strength. As we have seen, if the rf field is treated as a perturbation in the impulse theory, so that (13)-(15) are expanded keeping only first-order terms in the field, then we recover the set of area-preserving equations (26). We also note from Fig. 1b that as a particle passes through resonance and receives an impulsive "kick", its guiding center abruptly changes, moving across the magnetic field lines. The existence of this transverse motion may be responsible for the non-area-preserving character of the impulse equations when viewed in the restricted phase space of the two variables (u,ϕ). In the Hamiltonian theory, this transverse motion (drift across field lines) is immediately averaged out.

Of course, the impulse approximation itself does violence to the

physics of the particle-field interaction which is actually continuous rather than impulsive. In particular, the calculation of Section 2B in I shows that the effective time in resonance t_e is large compared to a cyclotron period, contrary to the impulsive assumption. Also, one must resort to approximate methods to calculate the impulse V, relying on the assumptions in I, (9) and assuming that as the particle passes through resonance, the motion along field lines is unperturbed by the rf field. Furthermore, one finds for particles turning in resonance that $V \propto v_\perp^{2/3}$, and it is not clear, for example, in (11), whether v_{n+1} should appear in place of v_n, or perhaps some average of the two velocities.

In an attempt to answer these questions, we again consider the exact numerical calculation of Fig. 7, recognizing that here the calculations are difficult, since the spiraling-in rates may be very small, and thus difficult to observe. The spiraling-in rate for V constant in terms of resonance crossings is from (25), $\beta = 1/450$, such that for $n = 100$, the particles would spiral in by ~ 22%, which should be measurable. For P = 2/3 the spiraling-in rate is comparable to that found above, and should also be observed. From Fig. 7 we see that there is no perceptible spiraling-in. The deviation from the area preserving mapping is therefore sufficiently smaller than that predicted from the impulse approximation that it is not observed in the numerical example. As a more stringent check on this property we have also numerically calculated an orbit for a field strength twice as large, which was found to be just adiabatic. Here $\beta \cong 1/225$ (for V constant) and the integration was carried out for approximately 200 resonance crossings. According to the impulse approximation the orbit would have spiraled in to approximately 1/e of its initial amplitude. In fact

no spiraling-in was observed. We conclude that the mappings are either exactly area preserving, as predicted from the Hamiltonian theory, or else they deviate by a sufficiently small amount to be of no practical importance.

3. STOCHASTIC APPROXIMATION

Under certain conditions, the simplifying assumption can be made that the phase θ_n is not determined by (14), but is described by a random process. Then (13) describes u_{n+1} as a function of a random variable θ. For a given random process, one can then calculate such quantities as the mean and mean square values of the transverse velocity increment $u_{n+1} - u_n$. As a further simplification, it is often assumed that all values of θ are equally probable. This is the random phase assumption. With additional assumptions, it is possible to write a Fokker-Planck equation, describing the time evolution of an initial distribution of particle velocities, as the heating process proceeds.

A. Fokker-Planck Equation

We first investigate in what sense the evolution of the velocity distribution function can be described by a stochastic process. Clearly the motion in the two dimensional phase plane is deterministic. However, provided $u < u_s$, so that neither spiraling-in or closed orbits exist, it may be possible to express the evolution of $f(u,n)$, the distribution in u alone, in terms of a Markov process in u (WANG and UHLENBECK, 1945).

$$f(u,n) = \int f(u-\Delta u,0)\ P(u-\Delta u,n|u)\,d(\Delta u), \qquad (40)$$

where P is the conditional probability of a particle being at u if it were at $u-\Delta u$, n collisions earlier. All quantities in (40) are supposed

to be independent of phase. If we make the additional assumption that $n >> 1$ and that $\Delta u << u$; i.e., that there exists a collision number n such that

$$1 << n << u/\Delta u \tag{41}$$

then (40) can be written in the form of a Fokker-Planck equation.

To correctly account for the geometry of the heating process (u is the radius in a polar coordinate system, and not a cartesian coordinate), we transform the Fokker-Planck equation in two dimensional cartesian coordinates

$$\frac{\partial f}{\partial n} = -\frac{\partial}{\partial u_x}(B_x f) - \frac{\partial}{\partial u_y}(B_y f) + \frac{1}{2}\frac{\partial}{\partial u_x^2}(D_{xx} f) + \frac{1}{2}\frac{\partial}{\partial u_y^2}(D_{yy} f) + \frac{\partial^2}{\partial u_x \partial u_y}(D_{xy} f), \tag{42}$$

where u_x and u_y are the cartesian velocity coordinates, into polar coordinates (u,θ) (see ROSENBLUTH et al, 1957). We obtain

$$\frac{\partial f}{\partial n} = -\frac{1}{u}\frac{\partial}{\partial u}(uBf) + \frac{1}{2}\frac{1}{u}\frac{\partial^2}{\partial u^2}(uDf) \tag{43}$$

where the frictional coefficient is

$$B(u) = \frac{1}{n}\int \Delta u P(u-\Delta u, n|u)\, d(\Delta u) \tag{44}$$

and the diffusion coefficient is

$$D(u) = \frac{1}{n}\int (\Delta u)^2 P(u-\Delta u, n|u)\, d(\Delta u). \tag{45}$$

B. Validity of the Fokker-Planck Equation

Of course, $P(u-\Delta u, n|u)$ is a function of the initial phase distribution as well as the initial velocity $u-\Delta u$. However, we expect that a correlation "time" n_c (measured in number of collisions) exists, such that any reasonably smooth initial phase distribution relaxes to a uniform phase distribution after approximately n_c collisions. Provided n can be chosen considerably larger than n_c, P will be independent of the initial phase distribution. To estimate n_c, we use the Jacobian matrix of the mapping (13)-(15) with P = 0 to obtain

$$\Delta u_{n+1} = \Delta u_n - (\sin \phi)\Delta\phi_n$$
$$\Delta\phi_{n+1} = - R\, \Delta u_n + (1 - R \sin \phi)\Delta\phi_n, \tag{46}$$

where $R \approx 2\pi M/u^2$ and we have assumed $u >> 1$. Below the stochastic transition velocity u_s, R is greater than four. In the worst case, we assume that the initial phases are spread over a small interval $\Delta\phi(0)$, and that $\Delta u(0) = 0$. Provided $R >> 1$, the dominant terms in (46) then yield $\Delta\phi(n) \simeq R^n\, \Delta\phi(0)$ and $\Delta u(n) \simeq R^{n-1}\, \Delta\phi(0)$. Setting the phase spread $\Delta\phi(n)$ equal to 2π, we find

$$n_c = \ln[2\pi/\Delta\phi(0)]/\ln R, \tag{47}$$

showing the weak logarithmic dependence of n_c on the initial phase interval, and thus on the form of the initial phase distribution. In contrast, since $\Delta u(n_c) << u$, the velocity distribution remains constant while phase randomization occurs. Provided $n >> n_c$ and inequality (42) is satisfied, then the Fokker-Planck description of the time-evolution of f is valid,

and the Fokker-Planck coefficients B and D can be obtained from a random phase assumption.

For $u > u_s$, invariants exist which relate velocity and phase, independent of time. These regions cannot therefore be described by (40). In the sea surrounding the invariant curves the process may be Markoffian in u, but the random phase assumption is clearly not appropriate, as all phases are not available at a given velocity.

C. Frictional and Diffusion Coefficients

We now calcuate the frictional and diffusion coefficients, making the assumption that the random process is adequately described by the single step (n = 1) equations (13)-(15); ie, the effects of higher order phase correlations associated with the multi-step mapping equations are negligible. This assumption has been explored in some detail (LIEBERMAN and LICHTENBERG, 1971), where it is shown that if the single step mapping equations yield B or D = 0, then the multi-step equations must be used. This is not the case for the mapping considered here. Since we are interested in the evolution of f as a function of time t, not step number n, we rewrite (43) as:

$$\frac{\partial f}{\partial t} = -\frac{1}{u}\frac{\partial}{\partial u}(B'uf) + \frac{1}{2}\frac{1}{u}\frac{\partial^2}{\partial u^2}(D'uf), \tag{48}$$

where B' and D' are respectively the time rate of change of Δu and $(\Delta u)^2$ respectively, averaged over phases:

$$B'(u) = \tau_b^{-1}\frac{1}{2\pi}\int_0^{2\pi} d\theta \Delta u, \tag{49}$$

and

$$D'(u) = \tau_b^{-1} \frac{1}{2\pi} \int_0^{2\pi} d\theta (\Delta u)^2, \tag{50}$$

where Δu is given from (13) as

$$\Delta u = (u^2 + u^{-2P} + 2u^{1-P} \cos\theta)^{1/2} - u, \tag{51}$$

with τ_b obtained from (7). Introducing a normalized time $T = t/\tau$, where

$$\tau = \pi(\ell^2 + L^2)^{1/2} / V_o, \tag{52}$$

and transforming to a new distribution function $g = uf$, we obtain the Fokker-Planck equation in normalized form:

$$\frac{\partial g}{\partial T} = - \frac{\partial}{\partial u} (\hat{B} g) + \frac{1}{2} \frac{\partial^2}{\partial u^2} (\hat{D} g), \tag{53}$$

where $\hat{B} = \tau B'$ and $\hat{D} = \tau D'$. The integrals in (49) and (50) may be performed to yield

$$\hat{B} = (2/\pi) u^{1-P} Y(u) E[4u^{1-P} Y(u)^{-2}] - u^2 \tag{54}$$

$$\hat{D} = u^{-2P} - 2u\hat{B}, \tag{55}$$

where

$$Y(u) = u^{1+P} + 1, \tag{56}$$

and E is the Jacobian elliptic integral of the second kind. In Fig. 8, $\hat{B}$ and $\hat{D}$ are given as a function of u, for various values of P.

D. Numerical Integration

To study the behavior of the Fokker-Planck equation (53) for all velocities and times, one must resort to numerical integration. Using an explicit integration scheme (KELLER, 1960) and particle-conserving boundary conditions ($\hat{B}g = \frac{1}{2}\frac{\partial}{\partial u}(\hat{D}g)$ at $u = 0$), (53) has been numerically integrated for values of P equal to 0, $\frac{1}{2}$ and 1. $P = 0$ corresponds to the weak rf field case (turning far from resonance), while $P = \frac{1}{2}$ and $P = 1$ bracket the value of P for turning in the resonance zone, $P = 2/3$. As an initial condition on g, a delta function at $u = 0.4$ was assumed. The results of the numerical integration are shown as the solid curves in Fig. 9a for $P = 0$. We note that for large velocities, the distribution function function falls off as e^{-Ku}, slower than a Maxwellian.

In Fig. 9b, results are given (solid curves) for $P = 1/2$, corresponding to $V \propto v_{\perp R}^{-1/2}$. We plot g on a semilogarithmic scale against u^2. For large velocities, a Maxwellian tail is obtained, $g \propto e^{-Ku^2}$. In Fig. 9c, the calculation is repeated (solid curves) for $P = 1$, corresponding to $V \propto v_{\perp R}^{-1}$. We plot g on a semilogarithmic scale against u^3 to show the faster-than-Maxwellian falloff of the tail of the distribution function. In Fig. 10, the average energy per particle $\langle u^2(T) \rangle$ is plotted as a function of time T, (solid curves) for the three cases (a) $P = 0$, (b) $P = 1/2$, and (c) $P = 1$. We discuss these curves in detail in the next subsection.

E. Approximate Analytic Solution

In the high velocity region, the Fokker-Planck coefficients (54) and (55) can be expand for $u > > 1$ to yield

$$\hat{B} = \frac{1}{4} u^{-2P} \tag{57}$$

$$\hat{D} = \frac{1}{2} u^{-2P+1} . \tag{58}$$

As P is increased, the coefficients fall off rapidly with increasing velocity. We thus expect that the larger the value of P, the faster the tail of the distribution function falls off with increasing velocity, a conclusion verified by the numerical calculations of Figs. 9a, b, and c. Inserting the coefficients (57) and (58) into the Fokker-Planck equation (53), we find

$$\frac{\partial g}{\partial T} = \frac{1}{4} \frac{\partial}{\partial u} u \frac{\partial}{\partial u} (g u^{-2P}). \tag{59}$$

A solution to (59) is sought which is particle-conserving. As an initial condition on g, we assume $g(u,0) = 2\delta(u)$, corresponding to a group of cold particles in the mirror at $T = 0$. The solution to (59) with this initial condition is

$$g(u,T) = \frac{4}{2P+1} \frac{u^{2P}}{T} \exp[- \left(\frac{2}{2P+1} \right)^2 u^{2P+1}/T], \tag{60}$$

which can easily be verified by substitution in (59). These solutions, for $T = 20$ ($T = 17$ for $P = 0$), are plotted as the dashed curves in Figs. 9a, b and c, for $P = 0$, 1/2 and 1 respectively. The agreement between (60) and the exact numerical integration of (53) is excellent for $u \gtrsim 2$. The tail of the distribution function g is seen to have a velocity dependence $\propto \exp(-Ku^{2P+1})$.

The number of particles in the mirror N(T) is given by

$$N(T) = N(0) \int_0^\infty du\, g(u,T). \tag{61}$$

Introducing a change of variable from u to

$$x = \frac{1}{T} \left(\frac{2}{2P+1} \right)^2 u^{2P+1} \tag{62}$$

in the above integration, we obtain N(T) = N(0); ie, the particle-conserving character of solution (60) is verified.

The average energy per particle $\langle u^2(T) \rangle$ is

$$\langle u^2(T) \rangle = \int_0^\infty du u^2 g(u,T). \tag{63}$$

Inserting (62) into this expression yields

$$\langle u^2(T) \rangle = (2a)^{-4a}\, T^{2a} \int_0^\infty x^{2a} e^{-x} dx$$

$$= (2a)^{-4a}\, \Gamma(2a+1) T^{2a}, \tag{64}$$

where $a = (2P+1)^{-1}$ and Γ is the Gamma function. The time dependence of the average energy per particle for various values of P is summarized in the table below.

P	a	$\langle u^2(T) \rangle$
0	1	$.125T^2$
1/2	1/2	T
2/3	3/7	$1.23T^{6/7}$
1	1/3	$1.55\ T^{2/3}$

These results for $\langle u^2(T) \rangle$ are plotted as the dashed lines in Figs. 10a, b and c for comparison with the results from the numerical integration (solid lines) of the Fokker-Planck equation (53). The agreement between the two is excellent, except for P = 0, where the initial energy in the numerical integration is larger than $.125T^2$, for $T \lesssim 2$.

We can also compare the stochastic theory for P = 0 with the numerical results of the impulse approximation in Section 2B. We see that the heating rate linearly proportional to time, obtained in (16) numerically from the mapping equations (13)-(15), without making a stochastic assumption, is in agreement with the heating rate obtained from (64), in which the assumption of random phases was made.

To estimate the magnitude of the average energy per particle W(t) which can be obtained in a typical pulsed experiment, (LICHTENBERG et al, 1969) we consider the case of P = 2/3 (turning in the resonance zone) with $\tau_{co} = 10^{-10}$sec, ℓ = 7.5 cm, L = 15 cm, and E = 10^3 V/cm. One finds $\tau_s = 4\text{x}10^{-10}$sec, and from (32), $V_o = 2.0\text{x}10^9$ cm/sec. Unnormalizing (64), we have

$$W(t) = 1.23\ W_o(t/\tau)^{6/7}, \tag{65}$$

where $W_o = \frac{1}{2} mV_o^2 = 1140$ eV, and τ is obtained from (52): $\tau = .26 \times 10^{-7}$ sec. For the rf pulse length $t = .25$ μsec of the experiment, one finds $W(t) = 9.7$ KeV, in excellent agreement with the approximately 8 KeV found experimentally.

We can compare the general results of the Fokker-Planck calculation with the exact numerical integration of the Lorentz force law for particles in the mirror. It is difficult, however to obtain adequate statistics from the numerical calculations, as it may take as long as 30 seconds of computer time per passage through resonance of a single particle. A numerical study was made corresponding to the electron cyclotron heating experiment by LICHTENBERG et al (1969), and we use the results of that study to compare with the theory.

In Fig. 11 we plot the average energy per particle $\langle W \rangle$ as a function of the resonance crossing n. The crosses are averages over four initial phases and the circles are averages for six initial phases. To compare the Fokker-Planck solutions with the numerical results we use the result that $n \propto W^{1/2} t$, which yields for the dependence $\langle W \rangle \propto t^{6/7}$ of (65) that $\langle W \rangle \propto n^{3/5}$. This dependence is plotted as a dashed line in Fig. 11 for n between 3 and 20, with an approximate joining of the result to the nonstochastic initial circle (n =1). (The energy after the first resonance crossing is deterministic, as the non phase dependent acceleration dominates for this first step.) The agreement between the stochastic theory for P = 2/3 and the exact orbit integrations is quite good.

We can also directly verify the random phase approximation for the exact orbit integrations by calculating the ratio of the cross corre-

lation to the autocorrelation for the phases at consecutive phase crossings,

$$\frac{\langle \sin \phi_{n+1} \sin \phi_n \rangle}{\langle \sin^2 \phi_n \rangle} \cong \frac{\frac{1}{n} \sum_{i=1}^{n} \sin \phi_{i+1} \sin \phi_i}{\frac{1}{n} \sum_{i=1}^{n} \sin^2 \phi_i} .$$

If the ratio approaches zero as $1/n^{1/2}$ for increasing n, then the phases can be considered random (MARGENAU and MURPHY, 1956). For a typical initial phase and n = 14 we obtained $\langle \sin \phi_{n+1} \sin \phi_n \rangle / \langle \sin^2 \phi_n \rangle = .16$ which is within the expected variance of $1/n^{1/2} = .27$.

4. CONCLUSION

We have presented in Section 2 an impulse approximation model of electron cyclotron resonance heating. The concept of impulsive heating in a localized zone about resonance was shown to be valid in I, with the strength of the transverse velocity impulse $V \propto v_{\perp R}^{-2/3}$, where $v_{\perp R}$ is the transverse particle velocity at resonance. Using this result, we obtained the mapping equations (13)-(15) relating the transverse particle velocity and phase on successive resonance crossings. The mapping equations were solved numerically for ~50,000 crossings to obtain phase-plane plots, and solved analytically in the neighborhood of the fixed points of the mapping to study the stability of the mapping. Three distinct phase plane regions were observed. For low particle velocities $u < u_s$, with u_s given by (23), the particle motion is stochastic in nature, and all fixed points of the mapping are unstable. For an intermediate velocity region $u_s < u < u_b$, where $u_b \approx 2.2u_s$, stable fixed points exist, and invariant curves en-

circling these fixed points and stochastic regions intermingle. For $u > u_b$, invariant curves exist which form a barrier to further particle heating. The mapping equations are weakly non-area-preserving, so the invariant curves are not exactly closed, but slowly spiral in to the stable fixed points.

We have compared the impulse approximation with the Hamiltonian approximation in I and with exact numerical orbit calculations with generally good agreement. The frequencies and widths of the oscillations about stable fixed points are in good agreement. For a fixed rf field, the barrier to particle heating given by (34) is in good agreement with the Hamiltonian theory I, (71) and with the results of the orbit calculations. We are unable, unequivocally, to numerically resolve the question as to whether spiraling-in orbits (impulse approximation) or closed, invariant curves (Hamiltonian approximation in I) really exist; the predicted spiraling-in rates are, however, much larger than these observed numerically, indicating that the transformation is probably area preserving. For application to actual experimental situations, the question may not be of much practical significance.

In Section 3, we considered a stochastic approximation to electron cyclotron heating, replacing the mapping equations for particle phase (14) and (15) with a random phase assumption, and demonstrating its validity in the stochastic region of phase space $u < u_s$. Taking account of the cylindrical geometry in velocity space, a Fokker-Planck equation (53) was derived for particle heating, with the Fokker-Planck coefficients (54) and (55) obtained from the mapping equation for particle velocity (13). The Fokker-Planck equation was solved by direct numerical integration and in an approximate analytical treatment. We found that the particle distribution function

evolved in time as $g(v_{\perp R},t) \propto (v_{\perp R}^{2P}/t)\exp-[Kv_{\perp R}^{2P+1}/t]$, where from the theory in I, $P \simeq 2/3$. The average particle energy evolves as $\langle v_{\perp R}^2 \rangle \propto t^{2/(2P+1)}$. These results agree with exact numerical orbit calculations, with the numerical solution to the mapping equations (no random phase assumption) and with observations of heating in a pulsed, electron cyclotron heating experiment (LICHTENBERG et al, 1969).

Although we have specifically treated mirror-confined plasmas, the general results are applicable to any system with localized heating zones in which the particles repetitively return to the resonance zone. The results can therefore be applied to toroidal devices. The general formulas for limitations on stochastic heating, heating rates, etc. will differ from those derived here by small numerical factors, provided the time required to return to the heating zone τ_b and the effective time spent in the heating zone t_e are properly specified.

In the treatment in this paper, we have considered the rf heating field as given, and studied the response of particles to this known field. For electron cyclotron heating experiments, the rf heating field can generally be taken to be the vacuum field, provided the plasma frequency is less than the electron cyclotron frequency, a condition often satisfied in experiments (LICHTENBERG et al, 1969; SPROTT, 1971). For high density experiments, or applications to ion heating or to situations in which the rf fields are self-generated (for example, a single mode of fluctuation in a mirror machine, ROSENBLUTH, 1971), the self-consistent properties of the plasma must be considered.

Acknowledgements. -- We acknowledge the help of C. Luk in making some of the numerical computations. This work was supported by the

National Science Foundation under Grant GK-27538 and the Air Force Office of Scientific Research under Grant AFOSR-69-1754.

REFERENCES

ARNOLD V. I. (1963) Russian Math. Surveys 18, 9.

GRAWE H. (1969) Plasma Phys. 11, 151.

JAEGER F. and LICHTENBERG A. J. (1971) Ann. Phys. (N.Y.) ___, .

JAEGER F., LICHTENBERG A. J. and LIEBERMAN M. A. (1971) Plasma Phys ___, .

KELLER H. B. (1960) Mathematical Methods for Digital Computers, ed. A. Ralston and H. S. Wolf, J. Wiley and Sons, New York, Cha. 12.

LICHTENBERG A. J. SCHWARTZ M. J. and TUMA D. T. (1969) Plasma Phys. 11, 101.

LIEBERMAN M. A. and LICHTENBERG A. J. (1971) Phys. Rev. ___, .

MARGENAU H. and MURPHY A. M. (1956) The Mathematics of Physics and Chemistry, D. Van Nostrand Co., Cincinnati, Ohio, Cha. 13.

MOSER J. (1962) Nachr. Akad. Wiss. Göttingen, II. Math. Physik Kl 1.

SPROTT J. C. (1971) Phys. Fluids 14, 1795.

STOKER J. J. (1950) Nonlinear Vibrations in Mechanical and Electrical Systems, Interscience Pub. Inc., New York, Cha. 3.

ROSENBLUTH M. N. (1971) Private communication.

ROSENBLUTH M. N., MACDONALD W. M. and JUDD D. L. (1957) Phys. Rev. 107, 1.

WANG M.C. and UHLENBECK G. E. (1945) Rev. Mod. Phys. 17, 323.

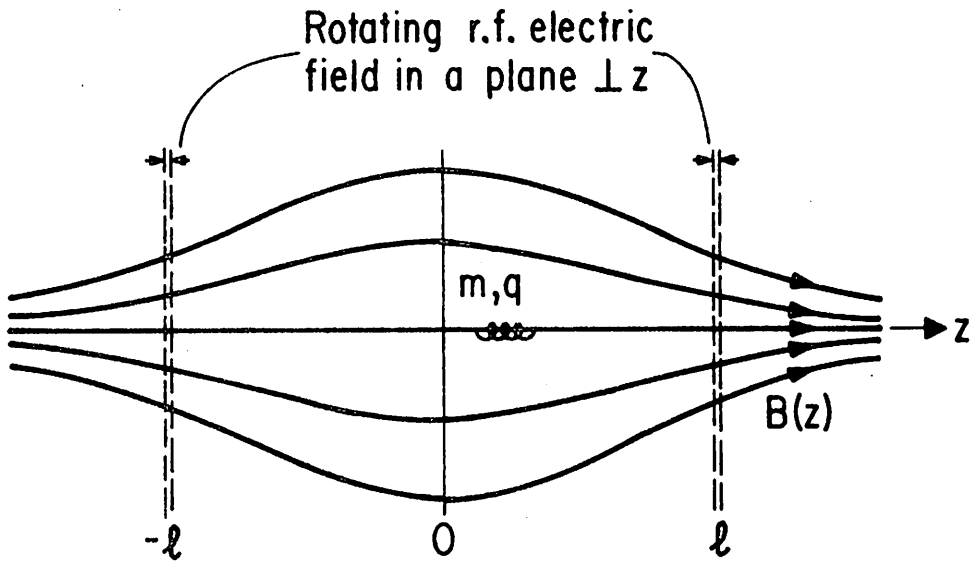

(a)

Fig. 1a. Cyclotron heating model in a magnetic mirror.

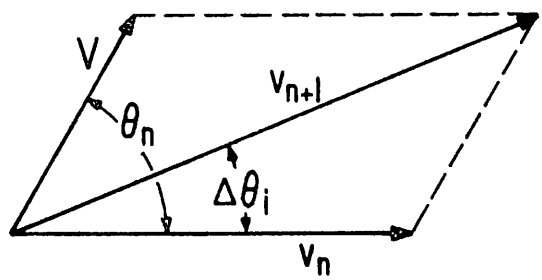

(b)

Fig. 1b. Geometrical relation between the velocities and phases in the resonance zone.

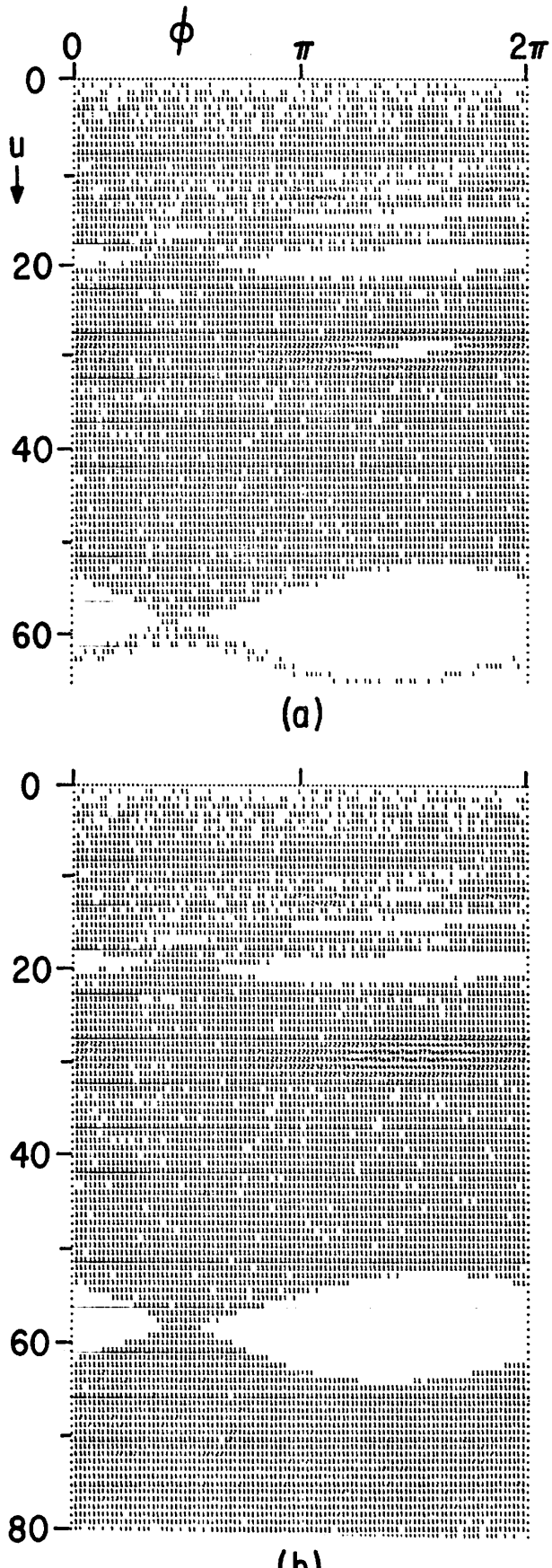

Fig. 2. Phase space (u,φ) for cyclotron heating. P = 0, M = 57.8, for 10 particles, after (a) 2560 and (b) 5120 collisions/particle.

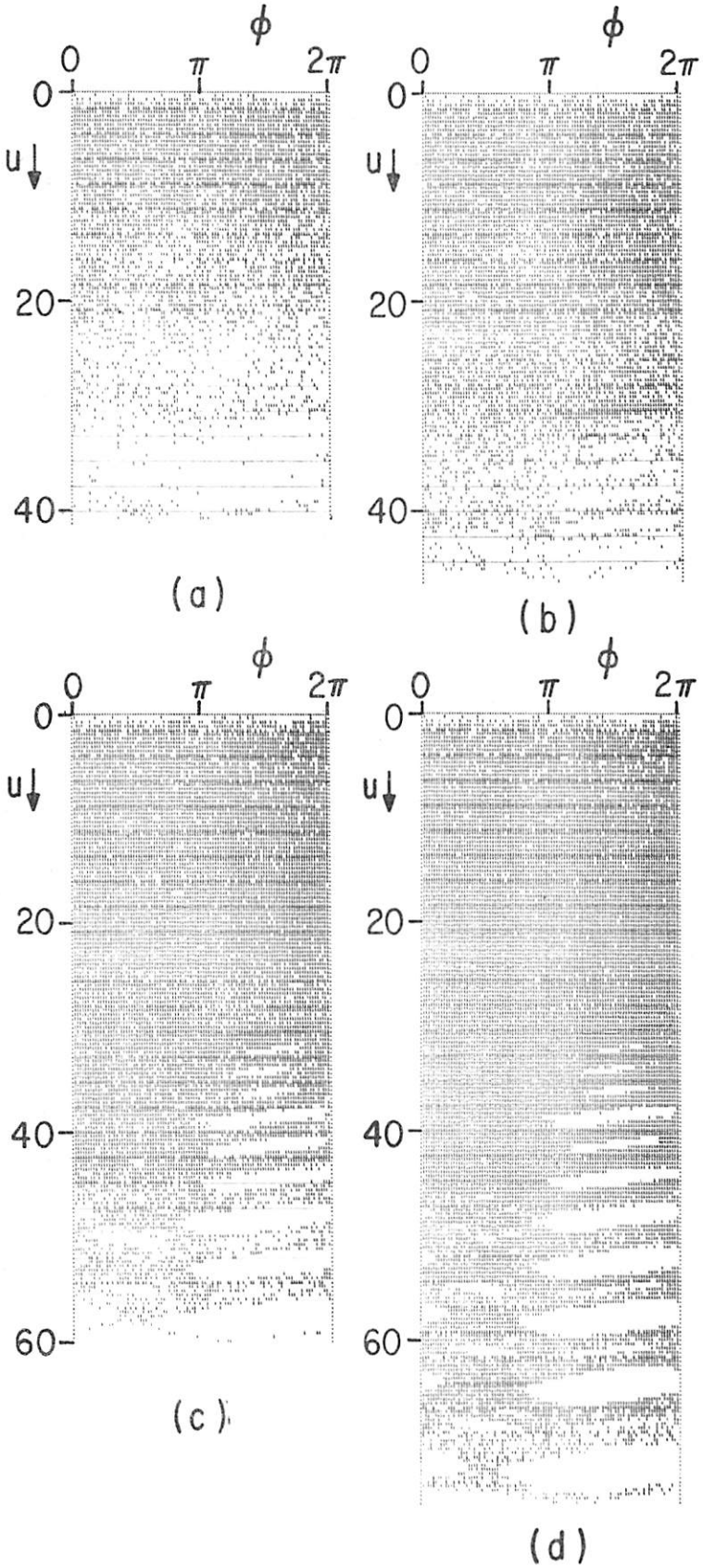

Fig. 3. Phase space (u,ϕ) for cyclotron heating. P = 0, M = 578, for 20 particles, after (a) 320, (b) 640, (c) 1280 and (d) 2580 collisions/particle.

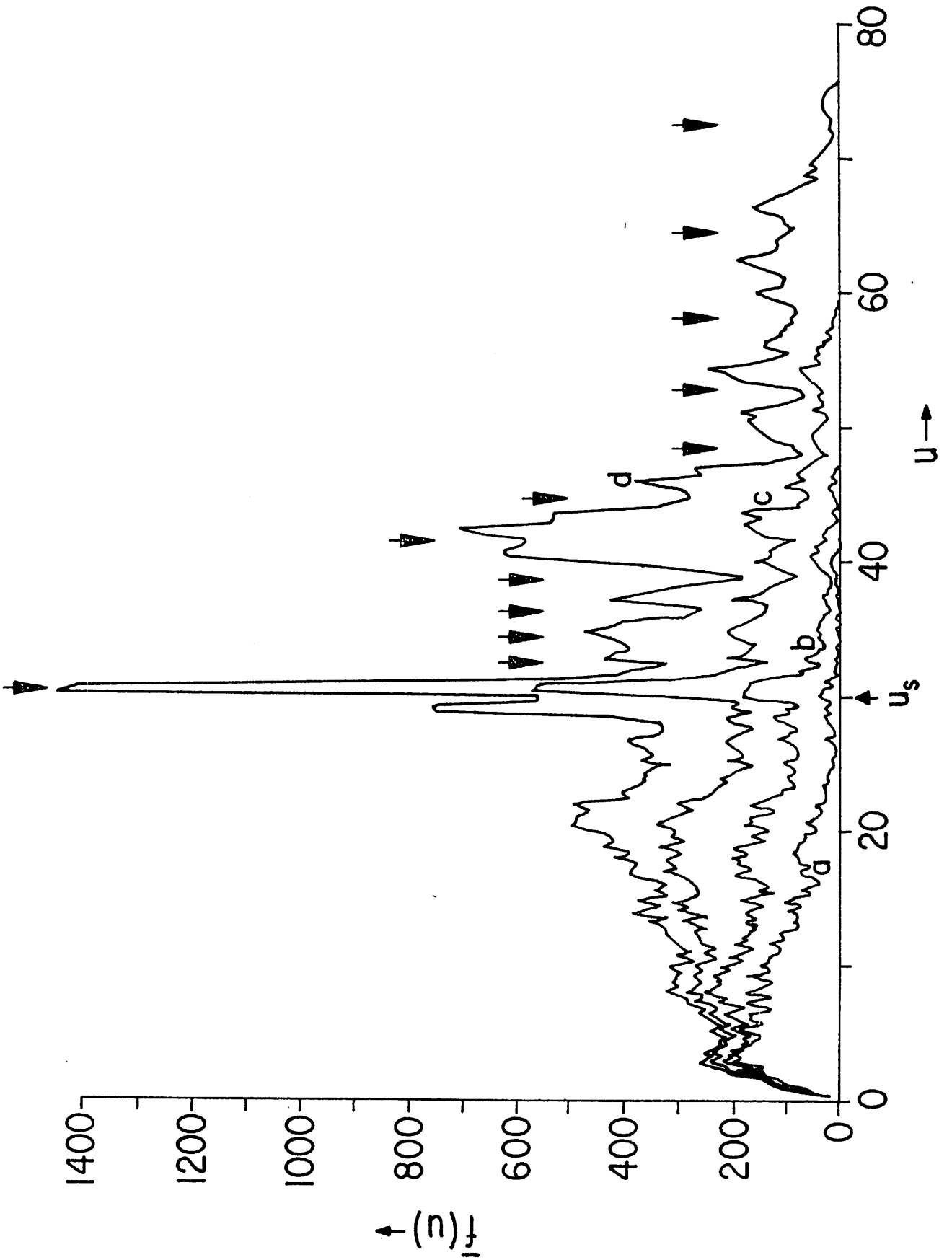

Fig. 4. The distribution function $\bar{f}(u)$ corresponding to the case of Fig. 3.

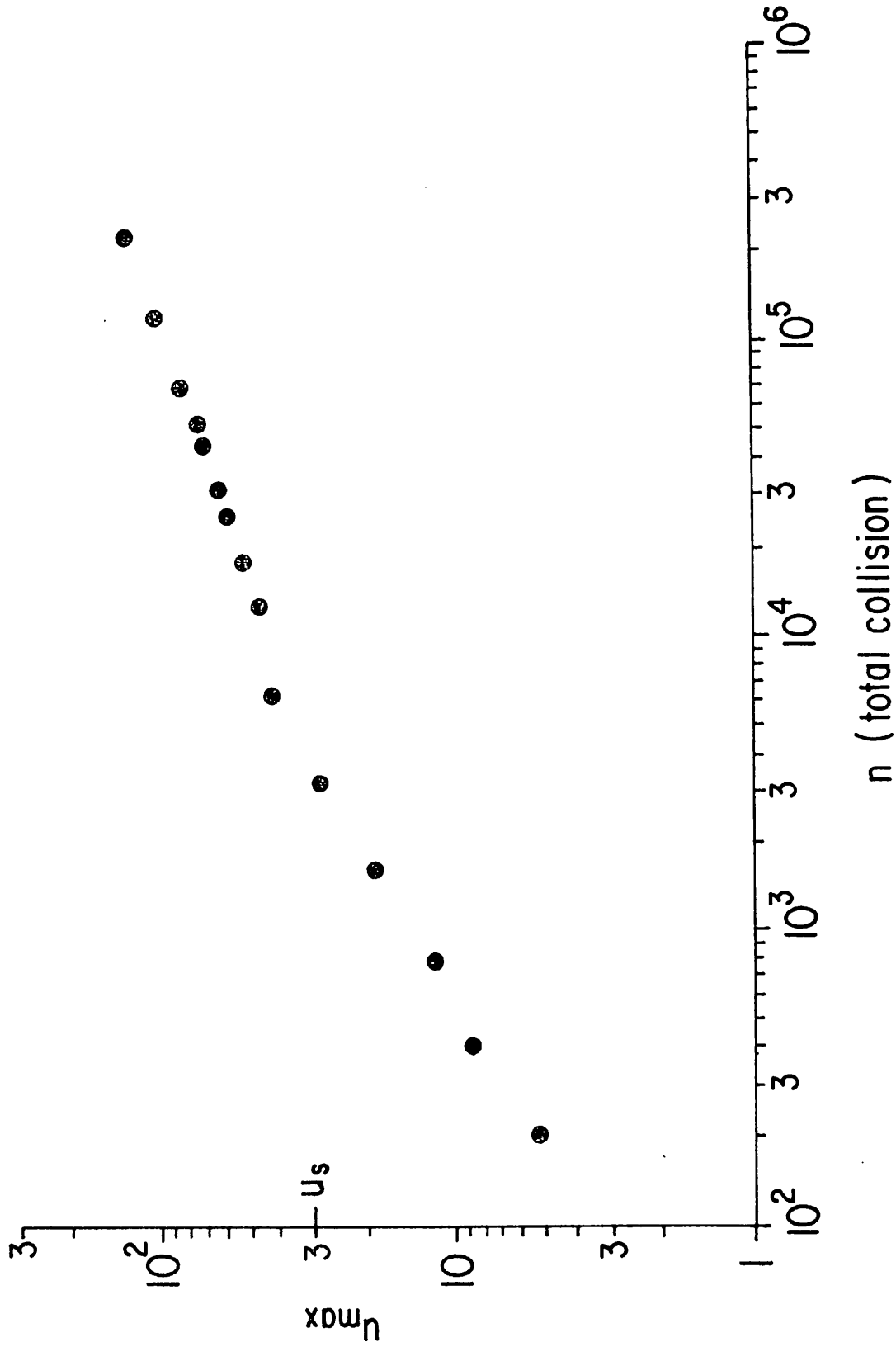

Fig. 5. Maximum velocity of a group of twenty particles vs. step number n, for the case of Fig. 3.

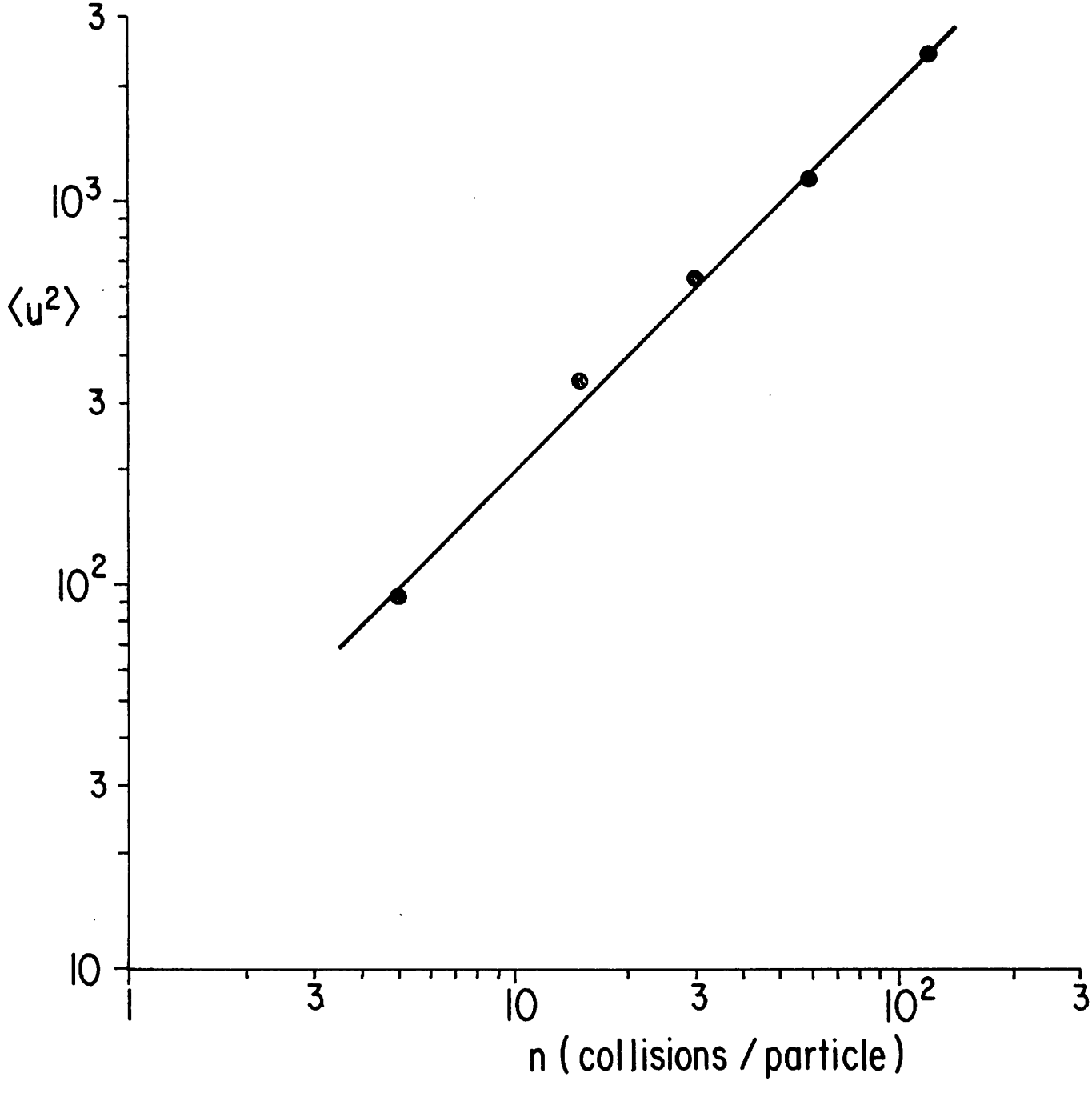

Fig. 6. Average energy $\langle u^2 \rangle$ vs. step number n, for the case of Fig. 3.

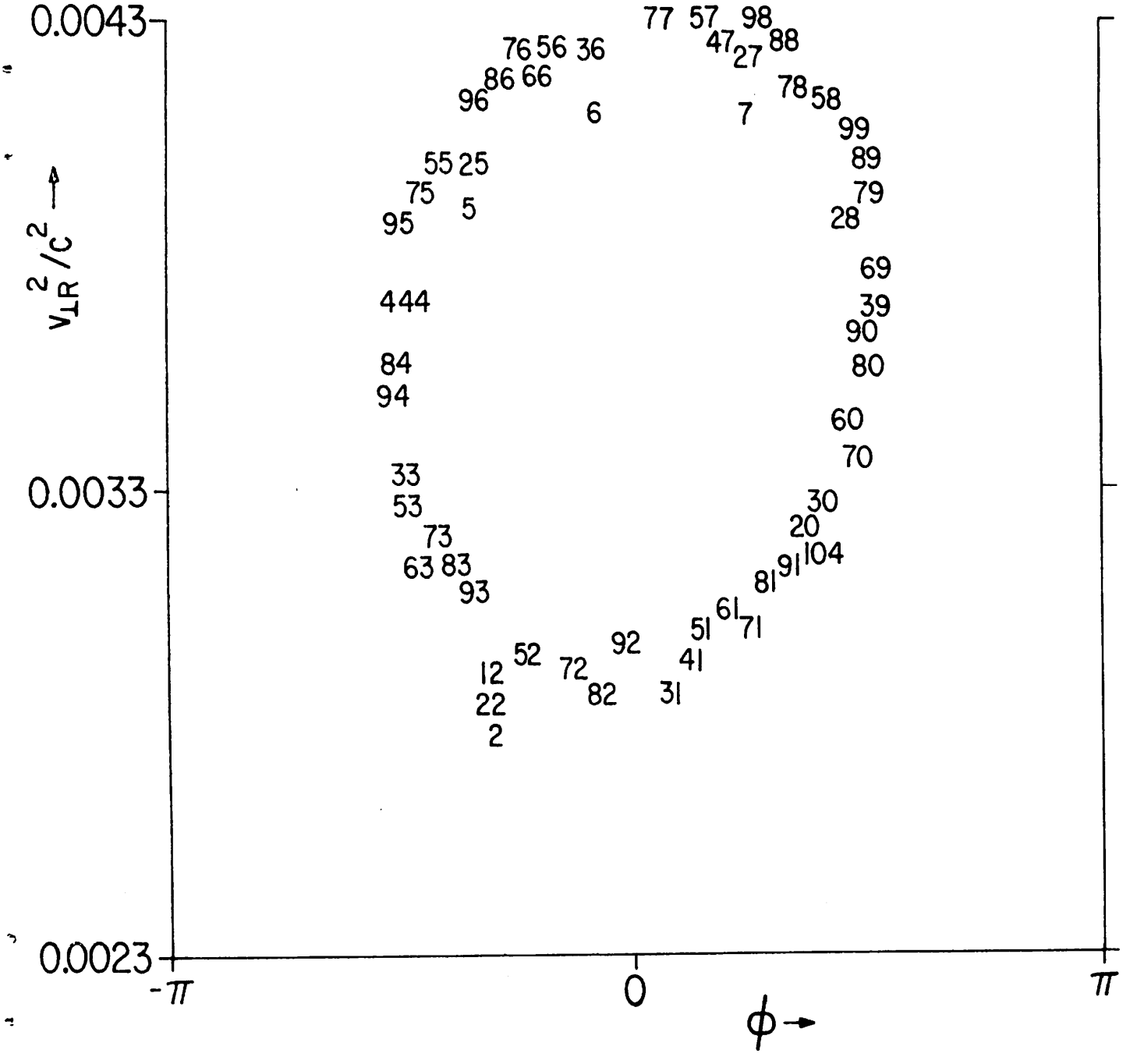

Fig. 7. Exact numerical calculation of phase space plot ($v_{\perp R}/c, \phi$) for M = 30, u = 15, corresponding to the m = 2 resonance. Successive resonance crossings are shown as successively numbered points.

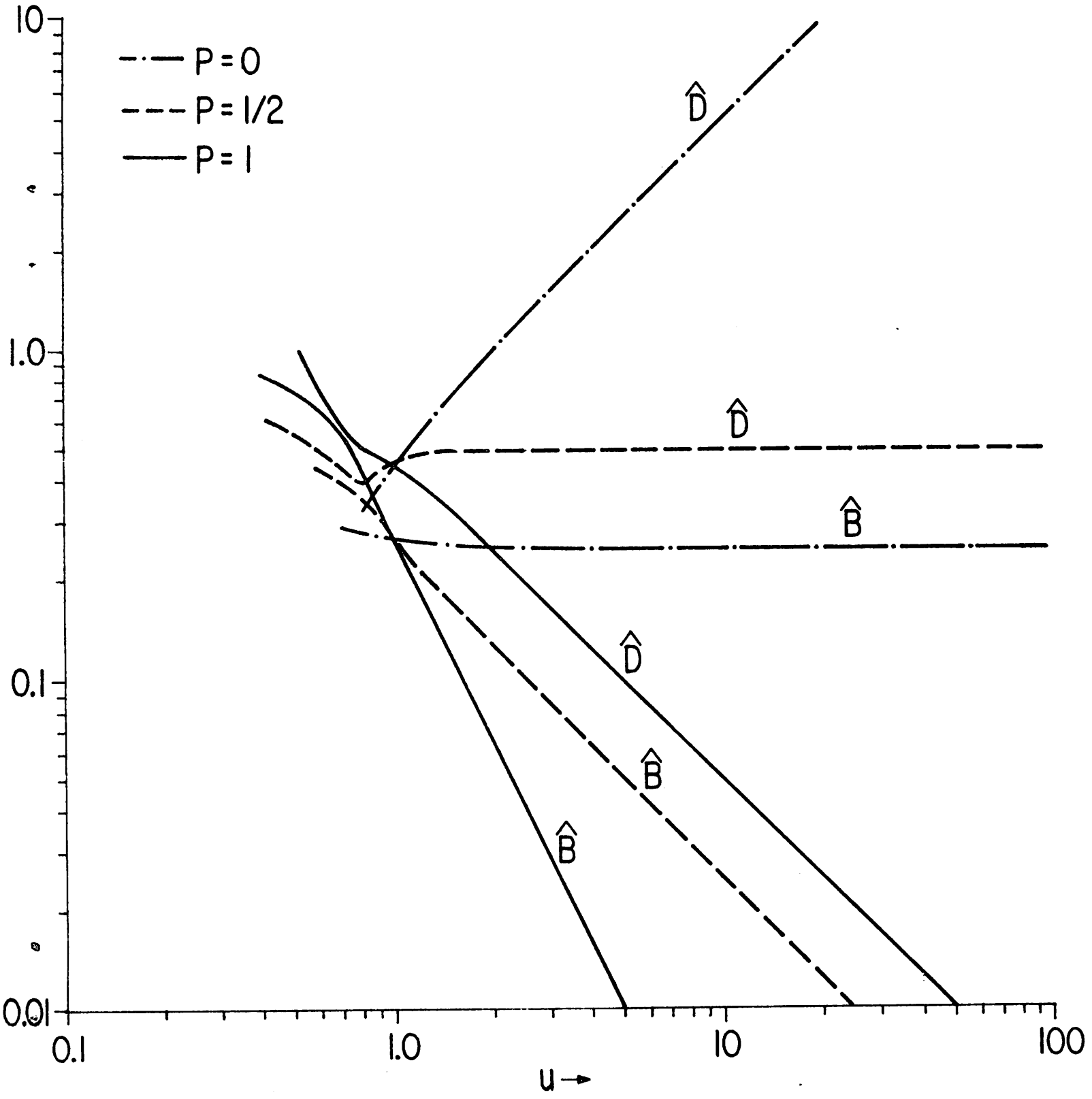

Fig. 8. Normalized Fokker-Planck coefficients $\hat{B}(u)$ and $\hat{D}(u)$ for P = 0, $\frac{1}{2}$ and 1.

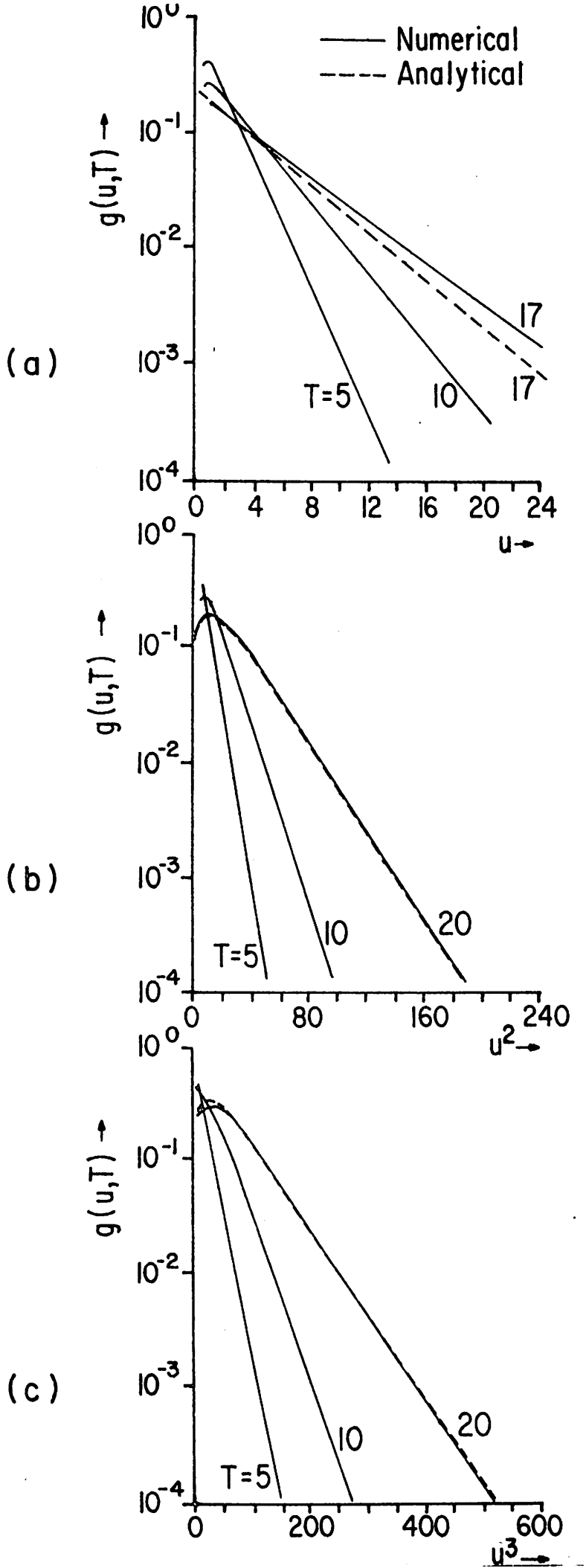

Fig. 9. g(u) vs. u at various times T, from numerical integration of the Fokker-Planck equation (solid lines) and from an analytical calculation valid for $u \gtrsim 2$ (dashed lines). (a) $P = 0$, (b) $P = \frac{1}{2}$ and (c) $P = 1$.

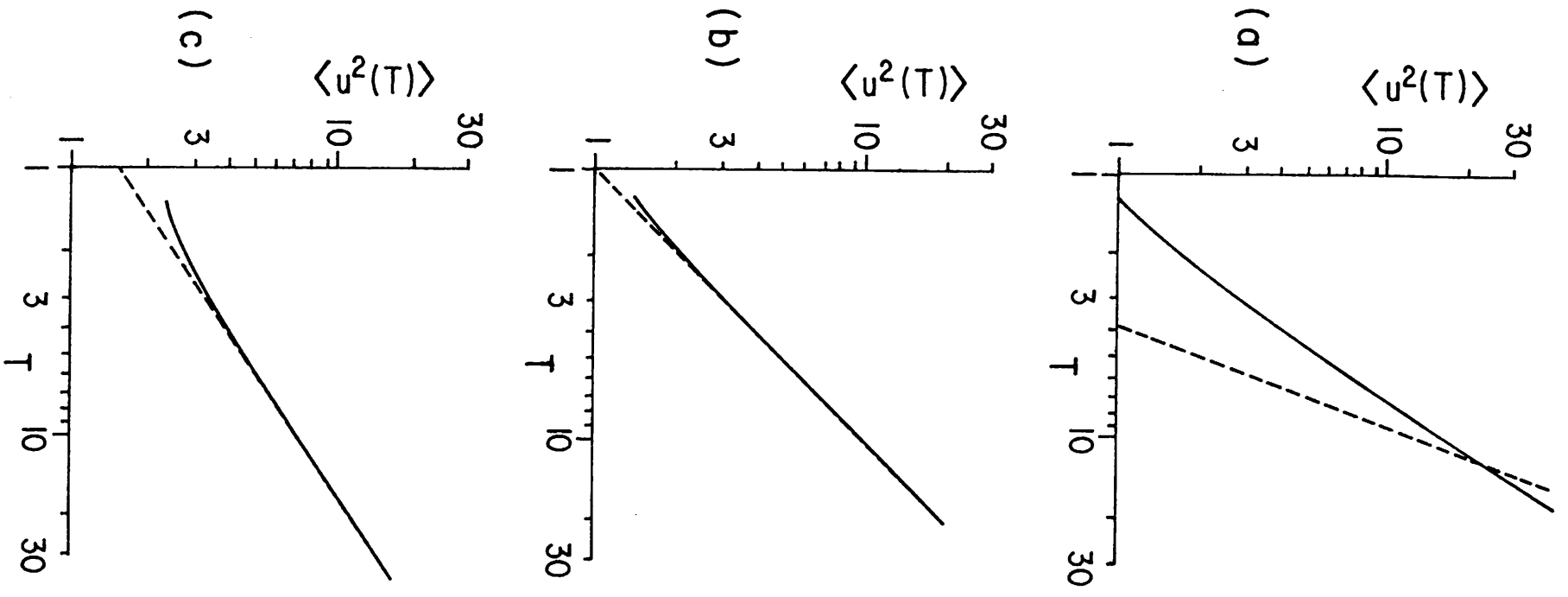

Fig. 10. Average energy per particle vs. time $\langle u^2(T) \rangle$ from numerical integration (solid lines) and from an analytical calculation valid for $u \gtrsim 2$ (dashed lines). (a) P = 0, (b) P = $\frac{1}{2}$ and (c) P = 1.

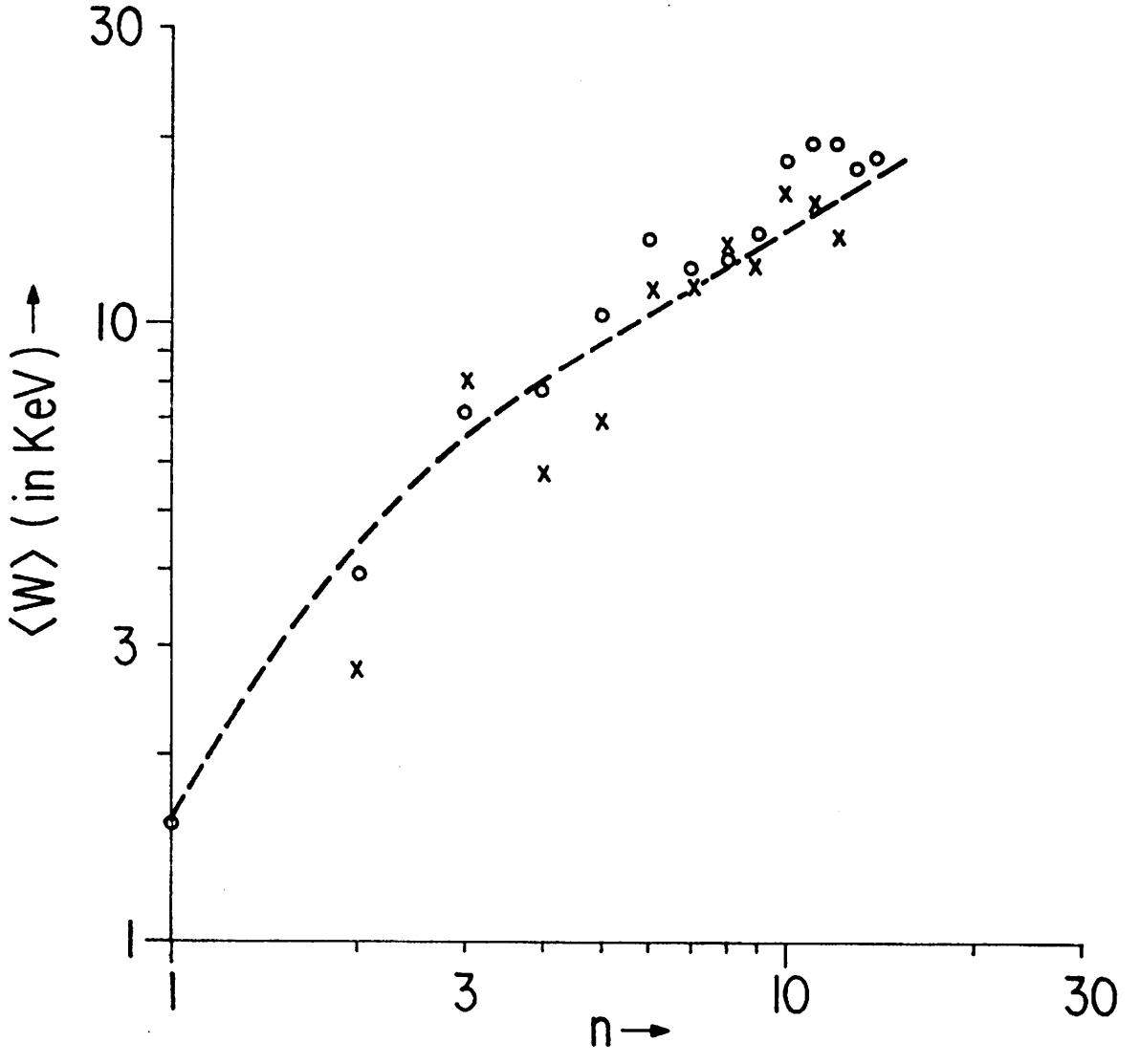

Fig. 11. Average energy per particle ⟨W⟩ vs. resonance crossing n, from exact numerical integration of the Lorentz force Law.